Geometric and nongeometric contributions to the surface anomalous Hall conductivity

Tomáš Rauch, Thomas Olsen, David Vanderbilt, and Ivo Souza

Phys. Rev. B **98**, 115108 — Published 5 September 2018

DOI: 10.1103/PhysRevB.98.115108

Geometric and nongeometric contributions to the surface anomalous Hall conductivity

Tomáš Rauch,[1] Thomas Olsen,[2] David Vanderbilt,[3] and Ivo Souza[1,4]

[1] *Centro de Física de Materiales, Universidad del País Vasco (UPV/EHU), 20018 San Sebastián, Spain*
[2] *CAMD, Department of Physics, Technical University of Denmark, 2820 Kgs. Lyngby Denmark*
[3] *Department of Physics and Astronomy, Rutgers University, Piscataway, New Jersey 08854-8019, USA*
[4] *Ikerbasque Foundation, 48013 Bilbao, Spain*

(Dated: August 16, 2018)

A static electric field generates circulating currents at the surfaces of a magnetoelectric insulator. The anomalous Hall part of the surface conductivity tensor describing such bound currents can change by multiples of e^2/h depending on the insulating surface preparation, and a bulk calculation does not fix its quantized part. To resolve this ambiguity, we develop a formalism for calculating the full surface anomalous Hall conductivity in a slab geometry. We identify a Berry-curvature term, closely related to the expression for the bulk anomalous Hall conductivity, whose value can change by quantized amounts by adjusting the surface Hamiltonian. In addition, the surface anomalous Hall conductivity contains a nongeometric part that does not depend on the surface preparation.

I. INTRODUCTION

Certain surface properties of crystals are strongly constrained by the bulk, and as a result they are very robust with respect to local perturbations. An example is the areal charge density $\sigma_{\rm surf}$ bound to an insulating surface of a polar insulator. For an unreconstructed defect-free surface with outward normal $\hat{\boldsymbol{n}}$ it is given by [1]

$$\sigma_{\rm surf} = \left(\boldsymbol{P} + \frac{e\boldsymbol{R}}{V_{\rm c}}\right)\cdot\hat{\boldsymbol{n}}, \tag{1}$$

where $\boldsymbol{P}$ is the bulk electric polarization, $\boldsymbol{R}$ is a lattice vector, and V_c is the volume of a unit cell. According to the Berry-phase theory [2], $\boldsymbol{P}$ is only defined modulo $e\boldsymbol{R}/V_{\rm c}$, since it is possible to change its value by that amount by adjusting the phases of the Bloch wave functions. Equation (1) assumes that a definite choice of gauge has been made so that a unique value of $\boldsymbol{P}$ has been established. (Here the word "gauge" refers to the freedom to adjust the phases of the Bloch eigenstates or, more generally, to perform a unitary transformation at each $\boldsymbol{k}$ among the occupied Bloch states [3].) The second term in Eq. (1) amounts to an integer number of electrons per surface unit cell. Its presence is required because it is in principle possible to prepare the insulating surface in different ways such that the macroscopic charge per surface cell changes by a multiple of the elementary charge e. Thus, the quantized part of $\sigma_{\rm surf}$ depends on the details at the surface but the nonquantized part does not.

In this work, we consider a similar situation that arises in insulating crystals that display the linear magnetoelectric (ME) effect, whereby an applied magnetic field $\boldsymbol{B}$ induces an electric polarization $\boldsymbol{P}$, and conversely an applied electric field $\boldsymbol{\mathcal{E}}$ induces a magnetization $\boldsymbol{M}$ [4, 5]. The linear ME tensor is defined as

$$\alpha_{ab} = \left.\frac{\partial P_a}{\partial B_b}\right|_{\boldsymbol{\mathcal{E}}=0} = \left.\frac{\partial M_b}{\partial \mathcal{E}_a}\right|_{\boldsymbol{B}=0}. \tag{2}$$

The full ME response contains both frozen-ion and lattice-mediated contributions, and each can be further decomposed into spin and orbital parts. In the following, we focus exclusively on the frozen-ion orbital response.

The bulk magnetization generated by a static electric field gives rise to surface currents

$$\boldsymbol{K} = \boldsymbol{M}\times\hat{\boldsymbol{n}}. \tag{3}$$

In the case of an insulating surface, this is the full current response. It is described at linear order by a 2×3 surface conductivity tensor $\sigma^{\rm surf}_{ab} = \partial K_a/\partial\mathcal{E}_b$, and the surface anomalous Hall conductivity (AHC) is defined as the antisymmetric part of the 2×2 block that describes the surface current generated by an in-plane electric field. Writing the surface AHC in vector form as $\sigma^{\rm AH}_{\rm surf}\,\hat{\boldsymbol{n}}$ where

$$\sigma^{\rm AH}_{\rm surf} = -\frac{1}{2}\epsilon_{cdb}\sigma^{\rm surf}_{cd}\hat{n}_b, \tag{4}$$

the surface anomalous Hall current density becomes

$$\boldsymbol{K}^{\rm AH} = \sigma^{\rm AH}_{\rm surf}\,\hat{\boldsymbol{n}}\times\boldsymbol{\mathcal{E}}. \tag{5}$$

From Eqs. (2) and (3) we find

$$\sigma^{\rm surf}_{cd} = \frac{\partial K_c}{\partial\mathcal{E}_d} = \frac{\partial}{\partial\mathcal{E}_d}\epsilon_{cea}M_e\hat{n}_a = \epsilon_{cea}\alpha_{de}\hat{n}_a, \tag{6}$$

and plugging this expression into Eq. (4) leads to

$$\sigma^{\rm AH}_{\rm surf} = -\frac{1}{2}{\rm Tr}(\alpha) + \frac{1}{2}\alpha_{ab}\hat{n}_a\hat{n}_b. \tag{7}$$

Separating the ME tensor on the right-hand side into an isotropic trace piece and a traceless part,

$$\alpha_{ab} = \alpha_{\rm iso}\delta_{ab} + \widetilde{\alpha}_{ab}, \tag{8}$$

we arrive at the relation

$$\sigma^{\rm AH}_{\rm surf} := -\alpha_{\rm iso} + \frac{1}{2}\widetilde{\alpha}_{ab}\hat{n}_a\hat{n}_b. \tag{9}$$

We use the special symbol := to indicate that while the left-hand-side is uniquely defined for a given surface termination, the right-hand side carries a quantum of indeterminacy, since the bulk quantity $\alpha_{\rm iso}$ is gauge invariant only modulo e^2/h [6, 7].

Once a definite value has been chosen for the multivalued quantity $\alpha_{\rm iso}$, Eq. (9) can be rewritten as

$$\sigma_{\rm surf}^{\rm AH} = -\alpha_{\rm iso} + m\frac{e^2}{h} + \frac{1}{2}\widetilde{\alpha}_{ab}\hat{n}_a\hat{n}_b. \tag{10}$$

Different choices of the integer m in the middle term correspond to different surface preparations exhibiting values of the surface AHC that differ by a multiple of the quantum of conductance.[1] This integer can be changed, in principle, by stitching a quantum anomalous Hall layer to the surface [7, 8] or otherwise changing the surface Hamiltonian, or by means of an adiabatic pumping cycle characterized by a nonzero second Chern number [10, 11]. It follows that only the nonquantized part of the surface AHC is a bulk property, in close analogy with Eq. (1) for the surface charge. These features are described by the phenomenology of axion electrodynamics [6, 12], and $\alpha_{\rm iso}$ is sometimes referred to as the axion ME coupling.

We are now ready to formulate the main question behind the present work. Suppose we have a ME insulator (it should break both inversion and time reversal symmetry), and we consider a specific insulating surface. How can we calculate the surface AHC, not just up to a quantum but exactly? Since we are given a definite surface Hamiltonian, there should be a definite answer without any quantum of ambiguity. We shall answer this question by developing a formalism that allows one to calculate the surface AHC unambiguoulsy using a slab geometry.

The manuscript is organized as follows. We begin in Sec. II by calculating, at linear order, the local current response of an insulator to a static homogeneous electric field. The local AHC, defined as the antisymmetric part of this local conductivity tensor, is then separated into geometric and nongeometric parts. Starting from the expression for the local AHC, we obtain in Sec. III an expression for the surface AHC of a slab, which we again separate into geometric and nongeometric parts. In Sec. IV we calculate numerically the surface AHC for slabs of tight-binding (TB) models and compare the results, via Eq. (10), with independent calculations of the bulk ME tensor. We conclude in Sec. V with a summary, and leave a lengthier derivation to an appendix.

[1] There are two scenarios compatible with Eq. (10). If the integer m is the same for all crystal facets, the entire surface is insulating and the term me^2/h gives an isotropic contribution to the surface AHC [8]. If adjacent facets have different m values, there are chiral conducting channels along the connecting hinges [9].

II. LOCAL ANOMALOUS HALL CONDUCTIVITY

A. Linear-response calculation

The local conductivity and local AHC are defined as

$$\sigma_{ab}(\boldsymbol{r}) = \left.\frac{\partial j_a(\boldsymbol{r})}{\partial \mathcal{E}_b}\right|_{\boldsymbol{\mathcal{E}}=0} \tag{11}$$

and

$$\sigma_c^{\rm AH}(\boldsymbol{r}) = -\frac{1}{2}\epsilon_{abc}\sigma_{ab}(\boldsymbol{r}), \tag{12}$$

respectively. $\boldsymbol{\mathcal{E}}$ denotes a static homogeneous electric field and $\boldsymbol{j}(\boldsymbol{r})$ is the microscopic induced current density, whose anomalous Hall part reads $\boldsymbol{j}^{\rm AH}(\boldsymbol{r}) = \boldsymbol{\sigma}^{\rm AH}(\boldsymbol{r}) \times \boldsymbol{\mathcal{E}}$.

We wish to calculate the local AHC for an insulating medium at zero temperature described by a single-particle Hamiltonian $\hat{H}$. The current operator is

$$\hat{\boldsymbol{j}}(\boldsymbol{r}) = -\frac{e}{2}\left(|\boldsymbol{r}\rangle\langle\boldsymbol{r}|\hat{\boldsymbol{v}} + \hat{\boldsymbol{v}}|\boldsymbol{r}\rangle\langle\boldsymbol{r}|\right), \tag{13}$$

where $\hat{\boldsymbol{v}} = (1/i\hbar)[\hat{\boldsymbol{r}}, \hat{H}]$ is the velocity operator and $e > 0$ is the elementary charge. The current density is given by

$$\boldsymbol{j}(\boldsymbol{r}) = \mathrm{Tr}\left[\hat{P}\hat{\boldsymbol{j}}(\boldsymbol{r})\right] = -e\,\mathrm{Re}\,\langle\boldsymbol{r}|\hat{\boldsymbol{v}}\hat{P}|\boldsymbol{r}\rangle, \tag{14}$$

where $\hat{P}$ denotes the projection operator onto the occupied states. An expression for the local conductivity (11) can now be obtained by differentiating Eq. (14) with respect to $\boldsymbol{\mathcal{E}}$. For that purpose we write $\hat{H} = \hat{H}_0 + e\boldsymbol{\mathcal{E}}\cdot\hat{\boldsymbol{r}}$ where $\hat{H}_0$ is the unperturbed Hamiltonian, and note that since $[\hat{r}_a, \hat{r}_b] = 0$ the operator $\hat{\boldsymbol{v}}$ reduces to $(1/i\hbar)[\boldsymbol{r}, \hat{H}_0]$. Hence the electric field enters Eq. (14) via $\hat{P}$ only,[2] leading to $\sigma_{ab}(\boldsymbol{r}) = (-e)\mathrm{Re}\,\langle\boldsymbol{r}|\hat{v}_a\partial_{\mathcal{E}_b}\hat{P}|\boldsymbol{r}\rangle$, and inserting this expression in Eq. (12) we arrive at

$$\boldsymbol{\sigma}^{\rm AH}(\boldsymbol{r}) = \frac{e}{2}\,\mathrm{Re}\,\langle\boldsymbol{r}|\hat{\boldsymbol{v}}\times\partial_{\boldsymbol{\mathcal{E}}}\hat{P}|\boldsymbol{r}\rangle. \tag{15}$$

Finally, from first-order perturbation theory we get

$$\partial_{\boldsymbol{\mathcal{E}}}\hat{P} = -e\sum_{v,c}\left(|c\rangle\frac{\langle c|\hat{\boldsymbol{r}}|v\rangle}{E_{cv}}\langle v| + |v\rangle\frac{\langle v|\hat{\boldsymbol{r}}|c\rangle}{E_{cv}}\langle c|\right), \tag{16}$$

where $|v\rangle$ and $|c\rangle$ denote occupied and empty energy eigenstates respectively, and $E_{cv} = E_c - E_v$. Equations (15) and (16) give the full local AHC; below, we separate it into geometric and nongeometric parts.

[2] We are ignoring local-field corrections, which introduce a dependence of $\hat{H}_0$ on $\boldsymbol{\mathcal{E}}$ through the self-consistent charge density. Such terms are not difficult to derive, but they are absent from our non-self-consistent TB calculations.

B. Separation of the local AHC into geometric and nongeometric parts

Consider the isotropic ME response of a bounded sample, defined as

$$\mathfrak{a}_{\rm iso} = \frac{1}{3}\sum_{a=1}^{3}\frac{\partial m_a}{\partial \mathcal{E}_a} \tag{17}$$

in terms of the orbital moment

$$\boldsymbol{m} = \frac{1}{2}\int \boldsymbol{r}\times\boldsymbol{j}(\boldsymbol{r})\,d^3r. \tag{18}$$

For a globally insulating crystallite of volume V, $\mathfrak{a}_{\rm iso}/V$ converges in the $V\to\infty$ limit to one of the multiple values of $\alpha_{\rm iso}$, with the specific value depending on the surface preparation [8]. Plugging Eq. (18) into Eq. (17) and comparing with the definition of the local AHC in Eq. (12) we find

$$\mathfrak{a}_{\rm iso} = -\frac{1}{3}\int \boldsymbol{r}\cdot\boldsymbol{\sigma}^{\rm AH}(\boldsymbol{r})\,d^3r. \tag{19}$$

This relation will be used below to isolate the geometric and nongeometric contributions to the local AHC, but first we need some results from the microscopic theory of the orbital ME response in insulators [13, 14].

The quantum-mechanical expression for the bulk ME tensor α_{ab} comprises an isotropic geometric term known as the Chern-Simons (CS) term, and a nongeometric term known as the Kubo or cross-gap (cg) term that has both isotropic and anisotropic parts [13, 14]. The relation between those two terms and the decomposition in Eq. (8) can be summarized as follows,

$$\alpha_{ab} = \underbrace{\big(\alpha_{\rm CS} + \overbrace{\alpha^{\rm cg}_{\rm iso}}^{\alpha^{\rm cg}_{ab}}\big)\delta_{ab} + \widetilde{\alpha}_{ab}}_{\alpha_{\rm iso}}. \tag{20}$$

The expressions for $\alpha_{\rm CS}$ and $\alpha^{\rm cg}_{ab}$ take the form of integrals over the Brillouin zone (BZ), and can be found in Refs. 13 and 14. In the case of $\alpha_{\rm CS}$ the integrand only contains the unperturbed cell-periodic Bloch functions and their first $\boldsymbol{k}$ derivatives. It is a gauge-dependent quantity, but after integration over the entire BZ it becomes gauge invariant modulo e^2/h. The expression for $\alpha^{\rm cg}_{ab}$ contains in addition the perturbed wavefunctions and the velocity operator, and is fully gauge invariant at each point in the BZ.

The ME tensor $\mathfrak{a}_{ab} = (\partial m_b/\partial\mathcal{E}_a)_{\boldsymbol{B}=0}$ of a finite crystallite can be similarly decomposed into geometric and nongeometric terms [13]. Because surface contributions are now included, the geometric part $\mathfrak{a}_{\rm CS}$ of the isotropic piece $\mathfrak{a}_{\rm iso}$ is unique for a given surface preparation. It is given by [13]

$$\begin{aligned}\mathfrak{a}_{\rm CS} &= -\frac{2\pi e^2}{3h}\epsilon_{abc}\,{\rm Im\,Tr}\left[\hat{P}_0\hat{r}_a\hat{P}_0\hat{r}_b\hat{P}_0\hat{r}_c\right]\\ &= \frac{2\pi e^2}{3h}\epsilon_{abc}\int r_c\,{\rm Im}\,\langle\boldsymbol{r}|\hat{P}_0\hat{r}_a\hat{Q}_0\hat{r}_b\hat{P}_0|\boldsymbol{r}\rangle\,d^3r,\end{aligned} \tag{21}$$

where $\hat{P}_0 = \sum_v |v\rangle\langle v|$ and $\hat{Q}_0 = \hat{\mathbb{1}} - \hat{P}_0$ are the ground-state projector and its complement, respectively. Comparing with Eq. (19), we are led to identify a geometric (CS) contribution to the local AHC given by

$$\boldsymbol{\sigma}^{\rm AH}_{\rm CS}(\boldsymbol{r}) = \frac{e^2}{h}\boldsymbol{C}(\boldsymbol{r}), \tag{22a}$$

$$\boldsymbol{C}(\boldsymbol{r}) = -2\pi{\rm Im}\,\langle\boldsymbol{r}|\hat{P}_0\hat{\boldsymbol{r}}\hat{Q}_0\times\hat{Q}_0\hat{\boldsymbol{r}}\hat{P}_0|\boldsymbol{r}\rangle. \tag{22b}$$

One can obtain the nongeometric (cross-gap) part of the local AHC in a similar way, starting from the nongeometric part of the orbital ME coupling of a crystallite. This is done in Appendix A, and as expected the result is that the cross-gap local AHC is equal to the difference between the full local AHC (15) and the CS term above,

$$\boldsymbol{\sigma}^{\rm AH}_{\rm cg}(\boldsymbol{r}) = \boldsymbol{\sigma}^{\rm AH}(\boldsymbol{r}) - \boldsymbol{\sigma}^{\rm AH}_{\rm CS}(\boldsymbol{r}). \tag{23}$$

Equations (15), (22), and (23) are the main results of this section.

C. Discussion

The appearence of a nongeometric term in the local AHC may seem surprising at first, since the intrinsic macroscopic AHC of a bulk crystal or slab is known to be purely geometric: it is given by the BZ integral of the Berry curvature of the occupied Bloch states [15]. The explanation, as we will see Sec. III D, is that the nongeometric term always integrates to zero across the full width of a slab, dropping out from the net AHC of the slab. As will become clear in the following, that term does contribute to the AHC of a single surface.

The nongeometric part of the local AHC was overlooked in some previous studies [7, 16], where the local AHC was formulated as a spatially-resolved Berry curvature. As for the geometric part, the expression in Eq. (22) is consistent with the previous literature. Consider a flat crystallite lying on the (x,y) plane, and integrate the quantity $C_z(\boldsymbol{r})$ given by Eq. (22b) over all z to obtain a dimensionless quantity $C_z(x,y)$. This is precisely the "local Chern number" introduced in Ref. 17. For a slab, the average of Eq. (22a) over a 2D cell at fixed z is essentially identical to the "layer-resolved AHC" of Ref. 7.

In the next section we calculate the layer-resolved AHC including both geometric and nongeometric contributions, and use it to evaluate the surface AHC.

III. SURFACE ANOMALOUS HALL CONDUCTIVITY

A. Evaluation in a slab geometry

Consider an insulating slab with the outward normal $\hat{\boldsymbol{n}} = \hat{\boldsymbol{z}}$ of the top surface pointing along a reciprocal-lattice vector $\boldsymbol{b}_3$. We assume that the slab thickness L is

much larger than the lattice constant $c = 2\pi/|\boldsymbol{b}_3|$ in the surface-normal direction. We also assume a defect-free surface, and introduce a "layer-resolved" AHC for the slab by averaging the z component of the local AHC (12) over a surface unit cell at fixed z,

$$\sigma^{\rm AH}_{\rm slab}(z) = \frac{1}{A_c}\int_{A_c} \sigma^{\rm AH}_z(x,y,z)\,dx\,dy. \tag{24}$$

The net AHC of a slab is given by

$$\sigma^{\rm AH}_{\rm slab} = \int \sigma^{\rm AH}_{\rm slab}(z)\,dz, \tag{25}$$

where the range of integration is chosen to span the full width of the slab, including the exponential tails of the wavefunctions outside the two surface regions. For an insulating slab the result is quantized in units of e^2/h [15],

$$\sigma^{\rm AH}_{\rm slab} = \frac{e^2}{h} C_{\rm slab}, \tag{26}$$

where the integer $C_{\rm slab}$ is the Chern number of the slab (see Sec. III D). In order for this equation to be meaningful, we are assuming that the slab is cut from a bulk insulator for which all three of the bulk Chern indices C_j [18] are zero.

As a first step towards calculating the surface AHC, we filter out the atomic-scale oscillations in the layer-resolved AHC by performing a "sliding-window average" over one vertical lattice constant,

$$\overline{\sigma}^{\rm AH}_{\rm slab}(z) = \frac{1}{c}\int_{z-c/2}^{z+c/2} \sigma^{\rm AH}_{\rm slab}(z')\,dz'. \tag{27}$$

Because we assumed $C_3 = 0$, this coarse-grained AHC must vanish exponentially in the bulklike interior region of the slab, and it can only become nonzero near the two surfaces. The macroscopic AHC of the top surface can now be expressed as

$$\sigma^{\rm AH}_{\rm surf} = \int_{z_0} \overline{\sigma}^{\rm AH}_{\rm slab}(z)\,dz, \tag{28}$$

with z_0 chosen in the bulklike region of the slab, and the upper limit of integration placed at an arbitrary point in the vaccum region above the top surface. The AHC of the bottom surface is $(e^2/h)C_{\rm slab} - \sigma^{\rm AH}_{\rm surf}$.

For numerical work, it is more convenient to recast Eq. (28) as

$$\sigma^{\rm AH}_{\rm surf} = \int \sigma^{\rm AH}_{\rm slab}(z) f_{\rm ramp}(z - z_0)\,dz, \tag{29}$$

where the range of integration spans the full width of the slab, and $f_{\rm ramp}$ is a ramp-up function defined as

$$f_{\rm ramp}(z) = \begin{cases} 0, \text{ for } z < -c/2 \\ z/c + 1/2, \text{ for } -c/2 < z < c/2 \\ 1, \text{ for } z > c/2 \end{cases}. \tag{30}$$

To summarize, Eq. (29) gives the surface AHC in terms of the layer-resolved AHC of Eq. (24), for which we provide an explicit formula below.

B. Layer-resolved anomalous Hall conductivity

We evaluate the layer-resolved AHC by inserting Eq. (15) for the local AHC into Eq. (24). The ground-state projector expressed in terms of the valence eigenstates of the slab reads

$$\hat{P}_0 = \frac{1}{N}\sum_{\boldsymbol{k}v} |\psi_{\boldsymbol{k}v}\rangle\langle\psi_{\boldsymbol{k}v}| \tag{31}$$

(the summation in $\boldsymbol{k} = (k_x, k_y)$ is over a uniform mesh of N points covering the surface BZ), and we need its linear change under an in-plane electric field,

$$\partial_{\boldsymbol{\mathcal{E}}}\hat{P} = \frac{1}{N}\sum_{\boldsymbol{k}v} e^{i\boldsymbol{k}\cdot\hat{\boldsymbol{r}}}\left(|\widetilde{\partial}_{\boldsymbol{\mathcal{E}}} u_{\boldsymbol{k}v}\rangle\langle u_{\boldsymbol{k}v}| + |u_{\boldsymbol{k}v}\rangle\langle\widetilde{\partial} u_{\boldsymbol{k}v}|\right) e^{-i\boldsymbol{k}\cdot\hat{\boldsymbol{r}}}. \tag{32}$$

Here $|u_{\boldsymbol{k}v}\rangle$ is the cell-periodic part of $|\psi_{\boldsymbol{k}v}\rangle$, and

$$|\widetilde{\boldsymbol{\partial}}_{\boldsymbol{\mathcal{E}}} u_{\boldsymbol{k}v}\rangle = ie\sum_c |u_{\boldsymbol{k}c}\rangle \frac{\hbar \boldsymbol{v}_{\boldsymbol{k}cv}}{E^2_{\boldsymbol{k}cv}} \tag{33}$$

is the projection of $|\boldsymbol{\partial}_{\boldsymbol{\mathcal{E}}} u_{\boldsymbol{k}v}\rangle$ onto the conduction bands, with $\boldsymbol{v}_{\boldsymbol{k}cv} = \langle u_{\boldsymbol{k}c}|\hat{\boldsymbol{v}}_{\boldsymbol{k}}|u_{\boldsymbol{k}v}\rangle$ and $\hat{\boldsymbol{v}}_{\boldsymbol{k}} = e^{-i\boldsymbol{k}\cdot\hat{\boldsymbol{r}}}\hat{\boldsymbol{v}}e^{i\boldsymbol{k}\cdot\hat{\boldsymbol{r}}}$. Equation (32) is essentially the same as Eq. (16), but adapted to a slab geometry. Putting everything together and letting $N \to \infty$ we arrive at

$$\sigma^{\rm AH}_{\rm slab}(z) = \frac{e}{4\pi h}\int d^2k \int_{A_c} dx\,dy \sum_v \mathrm{Re}\left[\langle\boldsymbol{r}|\hbar\hat{\boldsymbol{v}}_{\boldsymbol{k}} \times \left(|\widetilde{\boldsymbol{\partial}}_{\boldsymbol{\mathcal{E}}} u_{\boldsymbol{k}v}\rangle\langle u_{\boldsymbol{k}v}|\boldsymbol{r}\rangle + |u_{\boldsymbol{k}v}\rangle\langle\widetilde{\boldsymbol{\partial}}_{\boldsymbol{\mathcal{E}}} u_{\boldsymbol{k}v}|\boldsymbol{r}\rangle\right)\right]_z, \tag{34}$$

where the integral in $\boldsymbol{k}$ is over the surface BZ.

C. Separation of the layer-resolved AHC into geometric and nongeometric parts

To find the geometric part of the layer-resolved AHC we repeat the above steps, simply replacing Eq. (15) for

the full local AHC with Eq. (22) for the geometric part. Inserting Eq. (31) for $\hat{P}_0$ in Eq. (22b) gives

$$C_z(\boldsymbol{r}) = -\frac{4\pi}{N^2}\mathrm{Im}\sum_{\boldsymbol{k}\boldsymbol{k}'vv'}\psi^*_{\boldsymbol{k}v}(\boldsymbol{r})\psi_{\boldsymbol{k}'v'}(\boldsymbol{r})\langle\psi_{\boldsymbol{k}v}|\hat{x}\hat{Q}_0\hat{y}|\psi_{\boldsymbol{k}v}\rangle. \tag{35}$$

Writing $\hat{Q}_0$ as $(1/N)\sum_{\boldsymbol{k}c}|\psi_{\boldsymbol{k}c}\rangle\langle\psi_{\boldsymbol{k}c}|$ and using the identity $\langle\psi_{\boldsymbol{k}v}|\hat{r}_j|\psi_{\boldsymbol{k}'c}\rangle = iN\langle u_{\boldsymbol{k}v}|\partial_{k_j}u_{\boldsymbol{k}c}\rangle\delta_{\boldsymbol{k}\boldsymbol{k}'}$ valid for off-diagonal position matrix elements [19], we obtain

$$C_z(\boldsymbol{r}) = -\frac{4\pi}{N}\mathrm{Im}\sum_{\boldsymbol{k}}u^*_{\boldsymbol{k}v}(\boldsymbol{r})u_{\boldsymbol{k}v'}(\boldsymbol{r})F^{xy}_{\boldsymbol{k}v'v} \tag{36}$$

where

$$F^{xy}_{\boldsymbol{k}v'v} = \sum_c\langle\partial_{k_x}u_{\boldsymbol{k}v'}|u_{\boldsymbol{k}c}\rangle\langle u_{\boldsymbol{k}c}|\partial_{k_y}u_{\boldsymbol{k}v}\rangle = (\mathcal{F}^{yx}_{\boldsymbol{k}vv'})^* \tag{37}$$

is the metric-curvature tensor [3]. Inserting Eq. (36) in Eq. (22a) for $\boldsymbol{\sigma}^{\mathrm{AH}}_{\mathrm{CS}}(\boldsymbol{r})$ and plugging the result in Eq. (24) for the layer-resolved AHC yields, for $N\to\infty$,

$$\sigma^{\mathrm{AH}}_{\mathrm{slab,CS}}(z) = -\frac{e^2}{\pi h}\int\mathrm{Im}\,\mathrm{Tr}\,[\mathcal{O}_{\boldsymbol{k}}(z)F^{xy}_{\boldsymbol{k}}]\,d^2k. \tag{38}$$

The trace is over the valence bands, and

$$\mathcal{O}_{\boldsymbol{k}vv'}(z) = \int_{A_c}u^*_{\boldsymbol{k}v}(x,y,z)u_{\boldsymbol{k}v'}(x,y,z)\,dx\,dy \tag{39}$$

is a layer-resolved overlap matrix.

Equation (38) can be brought to a more transparent form by decomposing the metric-curvature tensor into Hermitean and anti-Hermitean parts in the band indices as $F^{xy}_{\boldsymbol{k}nm} = R^{xy}_{\boldsymbol{k}nm} + (1/2i)\widetilde{\Omega}^{xy}_{\boldsymbol{k}nm}$, where

$$R^{xy}_{\boldsymbol{k}nm} = \frac{1}{2}F^{xy}_{\boldsymbol{k}nm} + \frac{1}{2}\,(F^{xy}_{\boldsymbol{k}mn})^* \tag{40}$$

is the quantum metric and

$$\widetilde{\Omega}^{xy}_{\boldsymbol{k}nm} = iF^{xy}_{\boldsymbol{k}nm} + (iF^{xy}_{\boldsymbol{k}mn})^* \tag{41}$$

is the gauge-covariant Berry curvature, related to the Berry connection $A^a_{\boldsymbol{k}nm} = i\langle u_{\boldsymbol{k}n}|\partial_{k_a}u_{\boldsymbol{k}m}\rangle$ and to the non-covariant Berry curvature $\Omega^{xy}_{\boldsymbol{k}nm} = \partial_{k_x}A^y_{\boldsymbol{k}nm} - \partial_{k_y}A^x_{\boldsymbol{k}nm}$ by

$$\widetilde{\Omega}^{xy}_{\boldsymbol{k}nm} = \Omega^{xy}_{\boldsymbol{k}nm} - i\,[A^x_{\boldsymbol{k}}, A^y_{\boldsymbol{k}}]_{nm}\,. \tag{42}$$

Since the matrices $\mathcal{O}_{\boldsymbol{k}}(z)$, $R^{xy}_{\boldsymbol{k}}$, and $\widetilde{\Omega}^{xy}_{\boldsymbol{k}}$ are all Hermitean and the trace of the product of two Hermitean matrices is real, $R^{xy}_{\boldsymbol{k}}$ drops out from Eq. (38), which reduces to

$$\sigma^{\mathrm{AH}}_{\mathrm{slab,CS}}(z) = \frac{e^2}{2\pi h}\int\mathrm{Tr}\,\left[\mathcal{O}_{\boldsymbol{k}}(z)\widetilde{\Omega}^{xy}_{\boldsymbol{k}}\right]\,d^2k. \tag{43}$$

This expression for the CS layer-resolved AHC in terms of the layer-resolved overlap matrix and the non-Abelian Berry curvature is the central result of this section.

Equation (43), which essentially agrees with Eq. (12) of Ref. 7,[3] only accounts for part of the layer-resolved AHC, whose full amount is given by Eq. (34). According to Eq. (23) for the local AHC, the remainder is the non-geometric (or cross-gap) part of the layer-resolved AHC,

$$\sigma^{\mathrm{AH}}_{\mathrm{slab,cg}}(z) = \sigma^{\mathrm{AH}}_{\mathrm{slab}}(z) - \sigma^{\mathrm{AH}}_{\mathrm{slab,CS}}(z). \tag{44}$$

To review, the surface AHC is calculated from Eq. (29), where we insert either Eq. (34) to obtain the grand total, or Eq. (43) to find the geometric part.

D. Discussion

It was already mentioned in Sec. II C that although the nongeometric part of the layer-resolved AHC can give a net contribution to the surface AHC, its contribution to the AHC of the entire slab vanishes. To establish this result, let us show that the geometric part of the slab AHC coincides with the total.

We begin with the total slab AHC. Inserting Eq. (34) for the layer-resolved AHC into Eq. (25) yields

$$\sigma^{\mathrm{AH}}_{\mathrm{slab}} = -\frac{e^2}{2\pi h}\int d^2k\,\mathrm{Im}\sum_{vc}\frac{\hbar^2 v^x_{\boldsymbol{k}vc}v^y_{\boldsymbol{k}cv}}{E^2_{\boldsymbol{k}cv}} - (x\leftrightarrow y). \tag{45}$$

Using $\hbar\boldsymbol{v}_{\boldsymbol{k}vc} = -iE_{\boldsymbol{k}cv}\boldsymbol{A}_{\boldsymbol{k}vc}$ to remove the energy denominator and noting that $\mathrm{Im}\sum_{\boldsymbol{k}vv'}A^x_{\boldsymbol{k}vv'}A^y_{\boldsymbol{k}v'v} = 0$, the sum over conduction bands c can be replaced by a sum over all bands n (the term $n=v$ vanishes). Comparing with the Berry curvature $\Omega^{xy}_{\boldsymbol{k}v} = -2\mathrm{Im}\sum_{n\neq v}A^x_{\boldsymbol{k}vn}A^y_{\boldsymbol{k}nv}$ we arrive at Eq. (26) for the total slab AHC, with the slab Chern number given by [15]

$$C_{\mathrm{slab}} = \frac{1}{2\pi}\int d^2k\sum_v\Omega^{xy}_{\boldsymbol{k}v}. \tag{46}$$

To obtain the gometric part of the slab AHC, insert Eq. (42) into Eq. (43) and plug the result into Eq. (25). Using $\int\mathcal{O}_{\boldsymbol{k}vv'}(z)\,dz = \delta_{vv'}$ we get $\sigma^{\mathrm{AH}}_{\mathrm{slab,CS}} = C_{\mathrm{slab}}(e^2/h)$, which is the same as the total slab AHC. Thus, Eq. (44) must integrate to zero across the entire slab.

The net amount of AHC contributed by the cross-gap term (44) across a single surface region is equal to

$$\sigma^{\mathrm{AH}}_{\mathrm{surf,cg}} = -\alpha^{\mathrm{cg}}_{\mathrm{iso}} + \frac{1}{2}\widetilde{\alpha}_{ab}\hat{n}_a\hat{n}_b, \tag{47}$$

and the CS term (43) contributes the additional amount

$$\sigma^{\mathrm{AH}}_{\mathrm{surf,CS}} = -\alpha_{\mathrm{CS}} + m\frac{e^2}{h}. \tag{48}$$

Together, they make up the full surface AHC of Eq. (10).

[3] To obtain the expression in Ref. 7 for the CS layer-resolved AHC starting from the CS local AHC, one can repeat the derivation of Eq. (43) with a single modification: in Eq. (22b) for $C(\boldsymbol{r})$, exchange $\hat{P}_0$ and $\hat{Q}_0$ and remove the minus sign. It can be easily verified that this "particle-hole transformation" leaves $C(\boldsymbol{r})$ unchanged, as expected on physical grounds.

IV. NUMERICAL RESULTS

In the following we present the results of slab calculations of the surface AHC for two different TB models, and compare the results with bulk calculations of the orbital ME tensor [13]. First, let us briefly describe our TB implementation of the surface AHC expressions.

A. Tight-binding formulation of the surface AHC

In the TB context, the integration over z in Eq. (29) for the surface AHC gets replaced by a summation over a layer index l. The ramp-up function is evaluated at the discrete layer coordinates $z(l)$, and the layer-resolved AHC becomes $\sigma^{\rm AH}_{\rm slab}(l)$.

In Eq. (34) for the layer-resolved AHC, $|\boldsymbol{r}\rangle$ is replaced by $|i\rangle$ representing a TB orbital $\phi_i(\boldsymbol{r}) = \langle \boldsymbol{r}|i\rangle$, the integration $\int_{A_c} dx\, dy$ is replaced by a summation $\sum_{i\in l}$ over the orbitals within one surface unit cell in layer l, and the matrix elements of the velocity operator are evaluated by making the diagonal approximation $\langle i|\hat{\boldsymbol{r}}|j\rangle = \boldsymbol{\tau}_i \delta_{ij}$ for the position operator in the TB basis [20].

In Eq. (43) for the CS layer-resolved AHC the overlap matrix becomes

$$\mathcal{O}_{\boldsymbol{k}vv'}(l) = \sum_{i\in l} u^*_{\boldsymbol{k}v}(i)\, u_{\boldsymbol{k}v'}(i), \tag{49}$$

and the non-Abelian Berry curvature can be evaluated from Eqs. (37) and (41) with the help of the identity

$$\langle u_{\boldsymbol{k}c}|\partial_{\boldsymbol{k}} u_{\boldsymbol{k}v}\rangle = -\frac{\langle u_{\boldsymbol{k}c}|\hbar\hat{\boldsymbol{v}}_{\boldsymbol{k}}|u_{\boldsymbol{k}v}\rangle}{E_{\boldsymbol{k}cv}}. \tag{50}$$

B. Anisotropic cubic-lattice model

As our first test case, we consider a model of a ME insulator with no symmetry. This provides the most challenging case for the theory, since all nine components of the ME tensor are nonzero and different from one another. The resulting surface AHC has both CS and cross-gap contributions, and it varies with the surface orientation.

We choose the TB model described in Appendix A of Ref. 13. This is a spinless model defined on a cubic lattice, with one orbital per site and eight sites per cell, where inversion and time-reversal symmetry are broken by assigning random on-site energies and complex first-neighbor hoppings of fixed magnitude. We take the model parameters listed in Table A.1 of Ref. 13, and choose the two lowest bands to be the valence bands. As in that work, all parameters are kept fixed except for one hopping phase φ which is scanned from 0 to 2π, and the results are plotted as a function of this phase φ.

This model is intended as a model for a conventional ME insulator, in which the isotropic response $\mathfrak{a}_{\rm iso}/V$ of an insulating crystallite is very small relative to the quantum

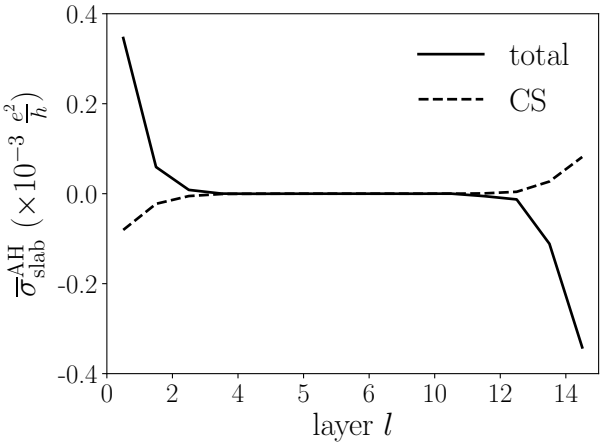

FIG. 1. Coarse-grained layer-resolved AHC [Eq. (51)] for a sixteen-atom-thick slab of the cubic-lattice model with $\varphi = \pi$.

e^2/h. The surface AHC of such a system is most naturally described by setting $m = 0$ in Eqs. (10) and (48) while choosing $\alpha_{\rm iso}$ and $\alpha_{\rm CS}$ in the range $[-e^2/2h, e^2/2h]$. (In the next subsection, we will consider a model with the opposite characteristics, i.e., with a large isotropic ME response of the order of e^2/h.)

We construct a slab with a thickness of sixteen atomic layers (eight lattice constants) along z. The layer-resolved AHC displays strong oscillations from one layer to the next, which we filter out by averaging over two consecutive layers,

$$\overline{\sigma}^{\rm AH}_{\rm slab}(l+1/2) = \frac{1}{2}\left[\sigma^{\rm AH}_{\rm slab}(l) + \sigma^{\rm AH}_{\rm slab}(l+1)\right]. \tag{51}$$

This quantity is plotted as the solid line in Fig. 1 for $\varphi = \pi$, and the dashed line shows the CS contribution the CS layer-resolved AHC was calculated for a different TB model in Ref. 7, and is shown in Fig. 2 therein). Both quantities are nonzero in the surface regions only, quickly dropping to almost zero within four subsurface layers. The fact that the two curves in Fig. 1 are not perfectly odd about the center of the slab can be attributed to the lack of mirror symmetry in the model. We have checked that both $\sum_l \sigma^{\rm AH}_{\rm slab}(l)$ and $\sum_l \sigma^{\rm AH}_{\rm slab,CS}(l)$ vanish identically, as should be the case for a slab with $C_{\rm slab} = 0$, so that the macroscopic surface AHC is equal and opposite for the two surfaces. On a given surface, the CS part of the AHC has the opposite sign compared to the total. The cross-gap contribution therefore prevails, as in ordinary ME insulators [8].

The macroscopic AHC of the top surface is plotted versus φ as the solid line in the top panel of Fig. 2, where the CS contribution is again shown as a dashed line. For comparison, we plot as filled (total) and empty (CS) circles the quantities on the right-hand side of Eqs. (10) and (48), respectively (with $m = 0$). The precise agreement validates our expression for the surface AHC, and its decomposition into geometric and nongeometric parts.

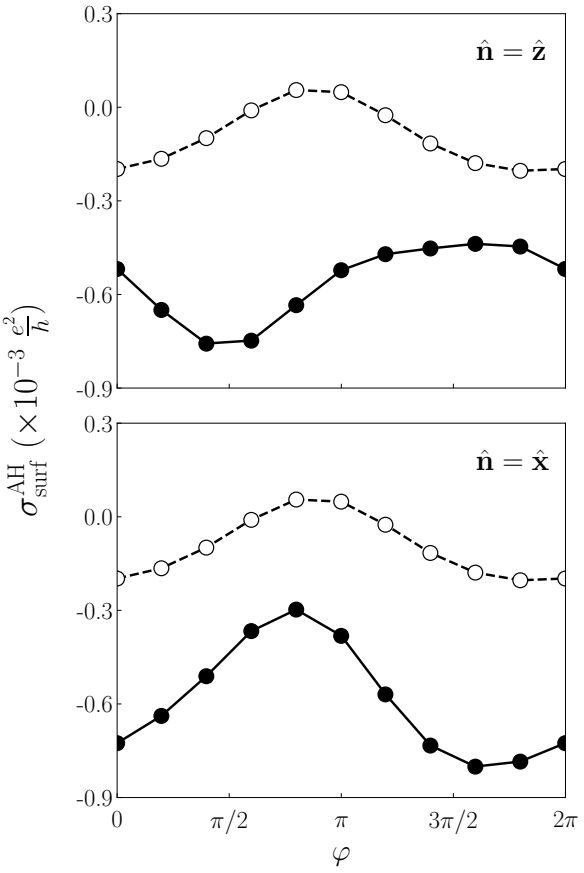

FIG. 2. AHC of the top surface (upper panel) and of the right surface (lower panel) of sixteen-layer slabs of the cubic-lattice model cut along z and x respectively, as a function of the cyclic parameter φ. The solid (dashed) lines denote the total (CS) surface AHC. Circles represent the quantity appearing on the right-hand-side of Eq. (9), with filled and empty circles denoting the total and the CS piece, respectively.

In the lower panel of Fig. 2 we show results for a slab cut along x. The total surface AHC is different from that on the upper panel, as expected for an anisotropic model from the last term in Eq. (47). The CS surface AHC is the same in both panels, confirming that its nonquantized part does not depend on the surface orientation, as expected from Eq. (48).

C. Layered Haldane model

We now turn to a model for which $\alpha_{\rm iso}$ and $\alpha_{\rm CS}$ are not always small compared to the quantum e^2/h, so that the branch choice in Eqs. (10) and (48) becomes ambiguous. We choose the TB model introduced in Ref. 11. This is a layered model on a hexagonal lattice, with four orbitals per cell. It can be obtained by stacking Haldane-model [21] layers with alternating parameters, and then coupling them via interlayer hopping terms. The model acts as a quantum pump of axion ME coupling: a slow

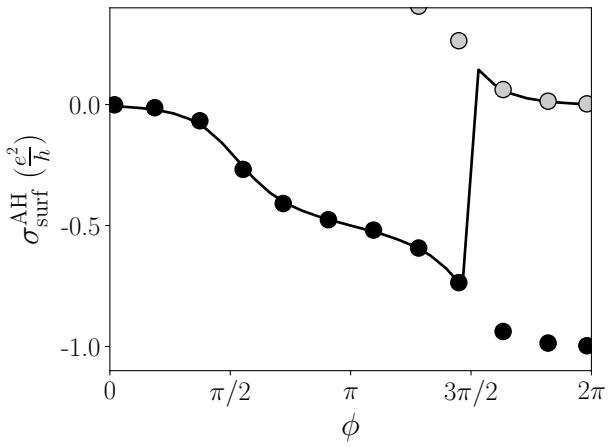

FIG. 3. Cyclic evolution of the Hamiltonian of a ten-layer slab of the layered Haldane model, during which the isotropic ME coupling $\alpha_{\rm CS}$ of the bulk crystal changes by e^2/h. The AHC of the top surface is plotted as a solid line, and the black and grey circles denote two different branches of $-\alpha_{\rm CS}$. For a given choice of branch, Eq. (48) is satisfied throughout the cycle with the value of m increasing by one at $\phi_c = 3\pi/2$.

periodic variation in its parameters can gradually change $\alpha_{\rm iso}$ by e^2/h over one cycle. Below, we monitor the evolution of the surface AHC during one pumping cycle.

We begin by noting that the cross-gap contribution to the ME tensor vanishes identically for this model. The reason can be found in Ref. 14, where a set of conditions were derived under which $\alpha^{\rm cg}_{ab}$ vanishes in certain four-band models having some kind of particle-hole symmetry. Those conditions hold for several models proposed in the literature including the present one, so that the total surface AHC (10) reduces to the CS part (48).

We construct a slab containing ten hexagonal layers stacked along z. The pumping cycle is parametrized by an angle ϕ that modulates the model parameters according to Eqs. (57c) and (61) in Ref. 11. As in Sec. III.D of that work, we consider the situation where the entire slab, including the surfaces, returns to its initial state at the end of the cycle,

$$\hat{H}_{\rm slab}(\phi = 2\pi) = \hat{H}_{\rm slab}(\phi = 0). \tag{52}$$

The quantities $\sigma^{\rm AH}_{\rm surf}(\phi)$ and $-\alpha_{\rm CS}(\phi)$ are plotted in Fig. 3 as solid lines and filled circles, respectively; the latter is a multivalued quantity, and two different branches are shown as black and grey circles. Equation (48) assumes that a specific branch has been chosen, and we pick the one represented by the black circles. With that choice, Eq. (48) is satisfied with $m = 0$ for $0 < \phi < 3\pi/2$ and with $m = 1$ for $3\pi/2 < \phi < 2\pi$.

The actual value of m at each ϕ depends on the particular gauge choice, but the important point is that Eq. (48) cannot be satisfied keeping m fixed for all ϕ. Equation (52) implies $\sigma^{\rm AH}_{\rm surf}(\phi = 2\pi) = \sigma^{\rm AH}_{\rm surf}(\phi = 0)$, and the only way this can be reconciled with the pumping of

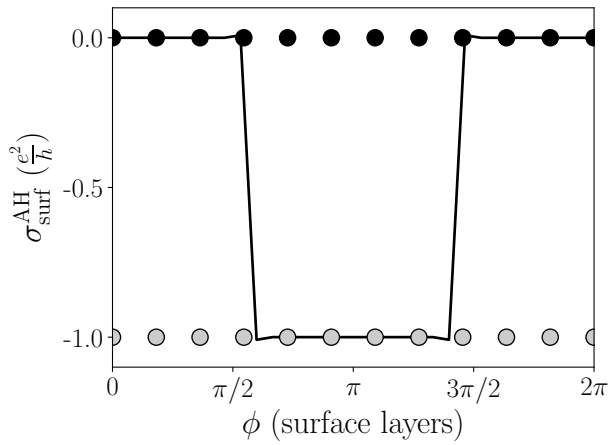

FIG. 4. The same quantities as in Fig. 3, but now for a cyclic evolution of the Hamiltonian of the surface layers only, keeping the Hamiltonian of the rest of the slab fixed.

CS axion coupling in the bulk region,

$$\alpha_{\rm CS}(\phi=2\pi)=\alpha_{\rm CS}(\phi=0)+\frac{e^2}{h}, \tag{53}$$

is if the integer m in Eq. (48) increases by one during the cycle. This change in the quantized part of the surface AHC is caused by a topological phase transition at the surface: the energy gap of the surface bands closes at $\phi_{\rm c}=3\pi/2$, forming a Weyl point in (k_x,k_y,ϕ)-space that transfers a quantum of Berry-curvature flux between the valence and conduction bands as ϕ crosses $\phi_{\rm c}$ [11].

It is also possible to change the quantized part of the surface AHC by adjusting only the surface Hamiltonian. This is illustrated in Fig. 4, where we held the Hamiltonian of all subsurface layers fixed at $\phi=0$, but modulated the onsite energy of the top and bottom layers by ϕ according to Eq. (57c) in Ref. 11. Now the bulk ME coupling $\alpha_{\rm CS}$ is held at zero for all ϕ, as indicated by the black circles. The surface AHC vanishes during half of the cycle leading to $m=0$ in Eq. (48), and it becomes $-e^2/h$ during the other half where $m=-1$. At the critical points $\phi_c=\pi/2$ and $\phi_c=3\pi/2$, the surface states become gapless.

V. SUMMARY

In this work we have derived practical expressions for calculating the full surface AHC of an insulating slab, including the quantized part that depends on the surface preparation. That quantized part resides in a geometric term written in terms of the gauge-covariant Berry curvature matrix of the slab wave functions. The full surface AHC contains an additional nongeometric term. Like the nonquantized part of the geometric surface AHC, that term is only apparently a surface property, but is in fact fully determined by the bulk ME tensor [13, 14].

Numerical TB calculations were carried out to show that our expressions satisfy the phenomenological relation in Eq. (10) between the surface AHC and the bulk ME coupling. The ability to change the surface AHC by multiples of e^2/h by adjusting the surface Hamiltonian was illustrated for a layered Haldane model.

The formalism developed in this work provides a simpler way of determining the quantized part of the surface AHC than an alternative approach based on hybrid Wannier functions [11]. It could be particularly useful for characterizing the nontrivial surface topology in second-order three-dimensional topological insulators with chiral hinge states [9, 22].

ACKNOWLEDGMENTS

This work was supported by the Forschungsstipendium RA 3025/1-1 from the Deutsche Forschungsgemeinschaft (T. R.), by Grant No. FIS2016-77188-P from the Spanish Ministerio de Economía y Competitividad (T. R. and I. S.), and by NSF Grant DMR-1629059 (D. V.).

Appendix A: Derivation of Eq. (23) for the cross-gap local AHC

The orbital moment (18) of a finite sample in a static electric field can be decomposed as [13]

$$\boldsymbol{m}(\boldsymbol{\mathcal{E}})=\boldsymbol{m}^{\rm CS}(\boldsymbol{\mathcal{E}})+\boldsymbol{m}^{\rm cg}(\boldsymbol{\mathcal{E}}), \tag{A1a}$$

$$\boldsymbol{m}^{\rm CS}(\boldsymbol{\mathcal{E}})=-\frac{2\pi e^2}{3h}\epsilon_{ijl}{\rm Im\,Tr}\left[\hat{P}\hat{r}_i\hat{P}\hat{r}_j\hat{P}\hat{r}_l\right]\boldsymbol{\mathcal{E}}, \tag{A1b}$$

$$m_i^{\rm cg}(\boldsymbol{\mathcal{E}})=\frac{\pi e}{h}\epsilon_{ijl}{\rm Im\,Tr}\left[\hat{P}\hat{r}_j\hat{Q}\hat{H}_0\hat{Q}\hat{r}_l-\hat{Q}\hat{r}_j\hat{P}\hat{H}_0\hat{P}\hat{r}_l\right]. \tag{A1c}$$

As in Sec. II A, $\hat{P}$ denotes the projection operator onto the occupied states in the presence of the field, $\hat{Q}=\hat{\mathbb{1}}-\hat{P}$, and $\hat{H}_0$ is the unperturbed Hamiltonian. Note that the CS term has an explicit linear dependence on $\boldsymbol{\mathcal{E}}$, while the cross-gap (cg) term only depends on $\boldsymbol{\mathcal{E}}$ implicitly via the projection operators. With the above decomposition, the isotropic ME coupling (17) becomes

$$\mathfrak{a}_{\rm iso}=\mathfrak{a}_{\rm iso}^{\rm CS}+\mathfrak{a}_{\rm iso}^{\rm cg}, \tag{A2}$$

with $\mathfrak{a}_{\rm iso}^{\rm CS}$ given by Eq. (21) and

$$\mathfrak{a}_{\rm iso}^{\rm cg}=-\frac{1}{3}\int r_i\epsilon_{ijl}\left.\frac{\partial T_j(\boldsymbol{r},\boldsymbol{\mathcal{E}})}{\partial\mathcal{E}_l}\right|_{\boldsymbol{\mathcal{E}}=0}d^3r, \tag{A3}$$

where

$$T_j(\boldsymbol{r},\boldsymbol{\mathcal{E}})=\frac{\pi e}{h}{\rm Im}\,\langle\boldsymbol{r}|\hat{P}\hat{r}_j\hat{Q}\hat{H}_0\hat{Q}-\hat{Q}\hat{r}_j\hat{P}\hat{H}_0\hat{P}|\boldsymbol{r}\rangle. \tag{A4}$$

Comparing Eq. (A3) with Eq. (19) for $\mathfrak{a}_{\rm iso}$ we conclude that the cross-gap local AHC is given by

$$\sigma^{\rm AH}_{{\rm cg},i}(\boldsymbol{r})=\epsilon_{ijl}\left.\frac{\partial T_j(\boldsymbol{r},\boldsymbol{\mathcal{E}})}{\partial\mathcal{E}_l}\right|_{\boldsymbol{\mathcal{E}}=0}. \tag{A5}$$

Our remaining task is to show that this expression is equivalent to Eq. (23).

We begin by plugging Eq. (A4) into Eq. (A5). This generates a total of six terms,

$$\sigma^{\mathrm{AH}}_{\mathrm{cg},i}(\boldsymbol{r}) = \frac{\pi e}{h}\epsilon_{ijl}\mathrm{Im}\,\langle\boldsymbol{r}|\Big[-\hat{P}_0\hat{r}_j\left(\hat{H}_0\hat{Q}_0\hat{P}_l\right) - \hat{P}_0\hat{r}_j\left(\hat{P}_l\hat{Q}_0\hat{H}_0\right) + \hat{P}_l\hat{r}_j\hat{H}_0\hat{Q}_0 \\ -\hat{Q}_0\hat{r}_j\left(\hat{H}_0\hat{P}_0\hat{P}_l\right) - \hat{Q}_0\hat{r}_j\left(\hat{P}_l\hat{P}_0\hat{H}_0\right) + \hat{P}_l\hat{r}_j\hat{H}_0\hat{P}_0\Big]|\boldsymbol{r}\rangle, \tag{A6}$$

where we used the fact that $\hat{H}_0$ commutes with both $\hat{P}_0$ and $\hat{Q}_0$, and introduced the notation $\hat{P}_l = \partial_{\mathcal{E}_l}\hat{P} = -\partial_{\mathcal{E}_l}\hat{Q}$ for the Cartesian components of $\partial_{\boldsymbol{\mathcal{E}}}\hat{P}$. Using Eq. (16) for that operator, the individual terms in Eq. (A6) become

$$-\mathrm{Im}\,\langle\boldsymbol{r}|\hat{P}_0\hat{r}_j\left(\hat{H}_0\hat{Q}_0\hat{P}_l\right)|\boldsymbol{r}\rangle = \frac{eE_c}{E_{cv}}\mathrm{Im}\,[\langle\boldsymbol{r}|v'\rangle\langle v'|\hat{r}_j|c\rangle\langle c|\hat{r}_l|v\rangle\langle v|\boldsymbol{r}\rangle], \tag{A7a}$$

$$-\mathrm{Im}\,\langle\boldsymbol{r}|\hat{P}_0\hat{r}_j\left(\hat{P}_l\hat{Q}_0\hat{H}_0\right)|\boldsymbol{r}\rangle = \frac{eE_c}{E_{cv}}\mathrm{Im}\,[\langle\boldsymbol{r}|v'\rangle\langle v'|\hat{r}_j|v\rangle\langle v|\hat{r}_l|c\rangle\langle c|\boldsymbol{r}\rangle], \tag{A7b}$$

$$\mathrm{Im}\,\langle\boldsymbol{r}|\hat{P}_l\hat{r}_j\hat{H}_0\hat{Q}_0|\boldsymbol{r}\rangle = -\frac{eE_{c'}}{E_{cv}}\mathrm{Im}\,[\langle\boldsymbol{r}|c\rangle\langle c|\hat{r}_l|v\rangle\langle v|\hat{r}_j|c'\rangle\langle c'|\boldsymbol{r}\rangle] - \frac{eE_{c'}}{E_{cv}}\mathrm{Im}\,[\langle\boldsymbol{r}|v\rangle\langle v|\hat{r}_l|c\rangle\langle c|\hat{r}_j|c'\rangle\langle c'|\boldsymbol{r}\rangle], \tag{A7c}$$

$$-\mathrm{Im}\,\langle\boldsymbol{r}|\hat{Q}_0\hat{r}_j\left(\hat{H}_0\hat{P}_0\hat{P}_l\right)|\boldsymbol{r}\rangle = \frac{eE_v}{E_{cv}}\mathrm{Im}\,[\langle\boldsymbol{r}|c'\rangle\langle c'|\hat{r}_j|v\rangle\langle v|\hat{r}_l|c\rangle\langle c|\boldsymbol{r}\rangle], \tag{A7d}$$

$$-\mathrm{Im}\,\langle\boldsymbol{r}|\hat{Q}_0\hat{r}_j\left(\hat{P}_l\hat{P}_0\hat{H}_0\right)|\boldsymbol{r}\rangle = \frac{eE_v}{E_{cv}}\mathrm{Im}\,[\langle\boldsymbol{r}|c'\rangle\langle c'|\hat{r}_j|c\rangle\langle c|\hat{r}_l|v\rangle\langle v|\boldsymbol{r}\rangle], \tag{A7e}$$

$$\mathrm{Im}\,\langle\boldsymbol{r}|\hat{P}_l\hat{r}_j\hat{H}_0\hat{P}_0|\boldsymbol{r}\rangle = -\frac{eE_{v'}}{E_{cv}}\mathrm{Im}\,[\langle\boldsymbol{r}|c\rangle\langle c|\hat{r}_l|v\rangle\langle v|\hat{r}_j|v'\rangle\langle v'|\boldsymbol{r}\rangle] - \frac{eE_{v'}}{E_{cv}}\mathrm{Im}\,[\langle\boldsymbol{r}|v\rangle\langle v|\hat{r}_l|c\rangle\langle c|\hat{r}_j|v'\rangle\langle v'|\boldsymbol{r}\rangle], \tag{A7f}$$

where a summation over repeated band indices is implied. We wish to bring the sum of all these terms into a "cross-gap" form, where dipole matrix elements only connect occupied and empty states. Four of the eight terms above already have that form and they can be combined in pairs, (A7a) with the second term in (A7f) and the first term in (A7c) with (A7d), to get

$$\frac{e(E_c+E_{v'})}{E_{cv}}\mathrm{Im}\,[\langle\boldsymbol{r}|v'\rangle\langle v'|\hat{r}_j|c\rangle\langle c|\hat{r}_l|v\rangle\langle v|\boldsymbol{r}\rangle] \\ + \frac{e(E_v+E_{c'})}{E_{cv}}\mathrm{Im}\,[\langle\boldsymbol{r}|c'\rangle\langle c'|\hat{r}_j|v\rangle\langle v|\hat{r}_l|c\rangle\langle c|\boldsymbol{r}\rangle]. \tag{A8}$$

In the remaining four terms, we use the completeness relation to bring them to the desired form. First we replace $|v'\rangle\langle v'|$ with $\hat{\mathbb{1}} - |c'\rangle\langle c'|$ in (A7b) and $|c'\rangle\langle c'|$ with $\hat{\mathbb{1}} - |v'\rangle\langle v'|$ in (A7e). The two terms containing $\hat{\mathbb{1}}$ can be reduced to

$$-r_j\mathrm{Im}\,[\langle\boldsymbol{r}|c'\rangle\langle c'|\hat{r}_l|c\rangle\langle c|\boldsymbol{r}\rangle] = 0, \tag{A9}$$

leaving

$$-\frac{eE_c}{E_{cv}}\mathrm{Im}\,[\langle\boldsymbol{r}|c'\rangle\langle c'|\hat{r}_j|v\rangle\langle v|\hat{r}_l|c\rangle\langle c|\boldsymbol{r}\rangle] \\ -\frac{eE_v}{E_{cv}}\mathrm{Im}\,[\langle\boldsymbol{r}|v'\rangle\langle v'|\hat{r}_j|c\rangle\langle c|\hat{r}_l|v\rangle\langle v|\boldsymbol{r}\rangle]. \tag{A10}$$

Next we combine the second term in (A7c) with the first in (A7f) using $\hat{H}_0 = E_{v'}|v'\rangle\langle v'| + E_{c'}|c'\rangle\langle c'|$,

$$\frac{e}{E_{cv}}\mathrm{Im}\,\left[\langle\boldsymbol{r}|\hat{H}_0\hat{r}_j|v\rangle\langle v|\hat{r}_l|c\rangle\langle c|\boldsymbol{r}\rangle + \langle\boldsymbol{r}|\hat{H}_0\hat{r}_j|c\rangle\langle c|\hat{r}_l|v\rangle\langle v|\boldsymbol{r}\rangle\right] \\ -\frac{e}{E_{cv}}\mathrm{Im}\,[E_{c'}\langle\boldsymbol{r}|c'\rangle\langle c'|\hat{r}_j|v\rangle\langle v|\hat{r}_l|c\rangle\langle c|\boldsymbol{r}\rangle + E_{v'}\langle\boldsymbol{r}|v'\rangle\langle v'|\hat{r}_j|c\rangle\langle c|\hat{r}_l|v\rangle\langle v|\boldsymbol{r}\rangle]. \tag{A11}$$

Writing $\hat{H}_0\hat{r}_j$ as $\hat{r}_j\hat{H}_0 - i\hbar\hat{v}_j$ and then cancelling two terms according to Eq. (A9), the first line becomes

$$-\frac{e\hbar}{E_{cv}}\mathrm{Re}\,[\langle\boldsymbol{r}|\hat{v}_j|v\rangle\langle v|\hat{r}_l|c\rangle\langle c|\boldsymbol{r}\rangle + \langle\boldsymbol{r}|\hat{v}_j|c\rangle\langle c|\hat{r}_l|v\rangle\langle v|\boldsymbol{r}\rangle]. \tag{A12}$$

Collecting terms in Eq. (A6) for the cross-gap local AHC we find, after some cancellations,

$$\sigma^{\rm AH}_{{\rm cg},i}(\boldsymbol{r}) = -\frac{e^2}{2E_{cv}}\epsilon_{ijl}{\rm Re}\,\left[\langle\boldsymbol{r}|\hat{v}_j|v\rangle\langle v|\hat{r}_l|c\rangle\langle c|\boldsymbol{r}\rangle + \langle\boldsymbol{r}|\hat{v}_j|c\rangle\langle c|\hat{r}_l|v\rangle\langle v|\boldsymbol{r}\rangle\right] + \frac{\pi e^2}{h}\epsilon_{ijl}{\rm Im}\,\left[\langle\boldsymbol{r}|v'\rangle\langle v'|\hat{r}_j|c\rangle\langle c|\hat{r}_l|v\rangle\langle v|\boldsymbol{r}\rangle - \langle\boldsymbol{r}|c'\rangle\langle c'|\hat{r}_j|v\rangle\langle v|\hat{r}_l|c\rangle\langle c|\boldsymbol{r}\rangle\right]. \tag{A13}$$

Comparing the first line with Eq. (16) for $\partial_{\boldsymbol{\mathcal{E}}}\hat{P}$ and using projection operators in the second line, we arrive at

$$\boldsymbol{\sigma}^{\rm AH}_{\rm cg}(\boldsymbol{r}) = \frac{e}{2}\,{\rm Re}\,\langle\boldsymbol{r}|\hat{\boldsymbol{v}}\times\partial_{\boldsymbol{\mathcal{E}}}\hat{P}|\boldsymbol{r}\rangle + \frac{\pi e^2}{h}{\rm Im}\,\left[\langle\boldsymbol{r}|\hat{P}_0\hat{\boldsymbol{r}}\hat{Q}_0\times\hat{Q}_0\hat{\boldsymbol{r}}\hat{P}_0|\boldsymbol{r}\rangle - \langle\boldsymbol{r}|\hat{Q}_0\hat{\boldsymbol{r}}\hat{P}_0\times\hat{P}_0\hat{\boldsymbol{r}}\hat{Q}_0|\boldsymbol{r}\rangle\right]. \tag{A14}$$

As noted earlier[3] the last two terms in this expression are equal to one another, resulting in Eq. (23).

[1] D. Vanderbilt and R. D. King-Smith, "Electric polarization as a bulk quantity and its relation to surface charge," Phys. Rev. B **48**, 4442 (1993).
[2] R. D. King-Smith and David Vanderbilt, "Theory of polarization of crystalline solids," Phys. Rev. B **47**, 1651 (1993).
[3] N. Marzari and D. Vanderbilt, "Maximally localized generalized Wannier functions for composite energy bands," Phys. Rev. B **56**, 12847 (1997).
[4] L. D. Landau and E. M. Lifshitz, *Electrodynamics of Continuous Media*, 2nd ed. (Pergamon Press, Oxford, 1984).
[5] M. Fiebig, "Revival of the magnetoelectric effect," J. Phys. D: Appl. Phys. **38**, R123 (2005).
[6] X.-L. Qi, T. L. Hughes, and S.-C. Zhang, "Topological field theory of time-reversal invariant insulators," Phys. Rev. B **78**, 195424 (2008).
[7] A. M. Essin, J. E. Moore, and D. Vanderbilt, "Magnetoelectric Polarizability and Axion Electrodynamics in Crystalline Insulators," Phys. Rev. Lett. **102**, 146805 (2009).
[8] S. Coh, D. Vanderbilt, A. Malashevich, and I. Souza, "Chern-Simons orbital magnetoelectric coupling in generic insulators," Phys. Rev. B **83**, 085108 (2011).
[9] M. Sitte, A. Rosch, E. Altman, and L. Fritz, "Topological Insulators in Magnetic Fields: Quantum Hall Effect and Edge Channels with a Nonquantized θ Term," Phys. Rev. Lett. **108**, 126807 (2012).
[10] M. Taherinejad and D. Vanderbilt, "Adiabatic Pumping of Chern-Simons Axion Coupling," Phys. Rev. Lett. **114**, 096401 (2015).
[11] T. Olsen, M. Taherinejad, D. Vanderbilt, and I. Souza, "Surface theorem for the Chern-Simons axion coupling," Phys. Rev. B **95**, 075137 (2017).
[12] F. Wilczek, "Two applications of axion electrodynamics," Phys. Rev. Lett. **58**, 1799 (1987).
[13] A. Malashevich, I. Souza, S. Coh, and D. Vanderbilt, "Theory of orbital magnetoelectric response," New J. Phys. **12**, 053032 (2010).
[14] A. M. Essin, A. M. Turner, J. E. Moore, and D. Vanderbilt, "Orbital magnetoelectric coupling in band insulators," Phys. Rev. B **81**, 205104 (2010).
[15] D. Xiao, M.-C. Chang, and Q. Niu, "Berry phase effects on electronic properties," Rev. Mod. Phys. **82**, 1959 (2010).
[16] A. Marrazzo and R. Resta, "Locality of the anomalous Hall conductivity," Phys. Rev. B **95**, 121114 (2017).
[17] R. Bianco and R. Resta, "Mapping topological order in coordinate space," Phys. Rev. B **84**, 241106 (2011).
[18] M. Kohmoto, B. I. Halperin, and Y.-S. Wu, "Quantized Hall effect in 3D periodic systems," Physica B **184**, 30 (1993).
[19] E. I. Blount, "Formalisms of Band Theory," Solid State Phys. **13**, 305 (1962).
[20] T. B. Boykin, "Current density and continuity in discretized models," Eur. Phys. J. **31**, 1077 (2010).
[21] F. D. M. Haldane, "Model for a quantum Hall effect without Landau levels: Condensed-matter realization of the "parity anomaly"," Phys. Rev. Lett. **61**, 2015 (1988).
[22] F. Schindler, A. M. Cook, M. G. Vergniory, Z. Wang, S. S. P. Parkin, B. A. Bernevig, and T. Neupert, "Higher-Order Topological Insulators," Sci. Adv. **4**, eaat0346 (2018).